Modelling the Evaporation of a Multicomponent Ellipsoidal Drop

Simona Tonini *, Gianpietro E. Cossali
[1]Department of Engineering and Applied Sciences, University of Bergamo, Italy
*Corresponding author: Simona.Tonini@unibg.it

Abstract
A model for heating and evaporation of non-spherical multicomponent drops is presented, based on the solution of energy and species conservation equations in orthogonal curvilinear coordinates, accounting also for the effect of convective conditions according to the film theory approach. The instantaneous evaporation rate of multicomponent drops is calculated as function of increased surface area due to drop deformation. The model is applied to spheroidal drops under quasi-steady and transient conditions, analysing the effect of drop size and velocity on the temperature evolution, for a range of drop and gas temperature operating conditions.

Introduction
The heat and mass transfer phenomena taking place when a liquid drop vaporises in a gaseous environment have been the subject of extensive research over many decades, due to their inherent interest in many engineering applications, like in spray combustion, spray cooling, spray drying, fire suppression, etc.
A wide literature became available in the latest years on the modelling of drop evaporation (see [1, 2] for recent reviews), analysing the complex physical phenomena involved.
The need to quantitatively predict such phenomena urged the development of models which on one hand have the capability of yielding reliable quantitative predictions of the heat and evaporation rates from a single drop, and on the other hand can be efficiently implemented in CFD codes to simulate dispersed flows. This need forced the introduction of many simplifying hypotheses, like constant properties of the gas mixture, quasi-steadiness, drop sphericity, homogeneous liquid temperature and composition, to cite some of the most common and stringent approximations [1].
After the simplest model for the mass transport from a particle immersed in a gas flow, proposed by Maxwell back in 1877 [3], exclusively based on mass diffusion mechanism, and the improvement reported in [4] to account for the importance of the Stefan flow, the model that better combines CPU efficiency, for dispersed flow applications, with a good quantitative accuracy is probably that of Abramzon and Sirignano [5], which was developed for spray combustion applications. Due to its numerical efficiency, it is nowadays commonly implemented in CFD codes for multi-drop calculations (particularly for sprays and aerosols).
Detailed numerical approach to the study of more complex physical aspects (drop composition, shape, interaction with other drops and/or solid surfaces (see [6, 7] for reference) are also available, but due to the complexity of the numerical implementation of these models and the CPU time requested for a single drop test case simulation, they cannot be used for multi-drop system predictions, but only as benchmarking for simpler models to be developed.
The above cited models were developed for single component drops, but the importance of understanding the phenomena taking place in multicomponent drop evaporation pressed the development of new models to relieve that limitation. A far less amount of literature is available on this more complex problem, since in this case the simultaneous diffusive–convective mass transfer from the drop to the gas cannot be simply modelled and/or experimentally studied. Important attempts can be found in [8-13].
The cited models all rely on the use of the Fick's law of diffusion, which is expected to hold only for dilute mixtures, and only recently an approach based on the solution of the Stefan-Maxwell equations, which relieves that limitation, was proposed in [14].
Parallel to the theoretical work, experimental work on multicomponent drop evaporation has considerably growth in the last years, as witnessed by many works available in the open literature (see [9, 15-17] to cite but a few).
The importance of taking into account the internal advection and diffusion was recognised, and again the necessity to develop CPU efficient models for implementation in CFD codes urged the introduction of an effective liquid conductivity and diffusivity of the liquid species, and analytical solution of the time dependent energy and conservation equations inside the liquid drop allowed to account for the effect of transport phenomena through the liquid drop [1].
The large number of component used in some applications (like in engine sprays) has driven the research to find method to simplify such multicomponent fuels by introducing the so called quasi-component [18] and the models has been applied to the simulation of Diesel, gasoline and bio-fuel droplets [9, 18-20].

All the available models dealing with multicomponent evaporation rely on the assumption that drop are spherical, thus allowing a simpler solution in spherical coordinates of the energy and species conservation equation. However, experimental investigation on liquid drops in multi-particle systems has revealed that they are subject to significant shape deformations while interacting with the carrier phase [21-23], due to the interaction of surface tension and fluid-dynamic stresses on the drop surface [23]. While surface tension force induces a spherical shape, fluid-dynamic forces are the primary sources of drop deformation. This is clearly evident in case of liquid drop with Weber number above 2, typical of spray combustion applications, which are appreciably non-spherical [22]. These observations were confirmed by numerical studies on liquid deformed drops [24], [25]. In [26] it was shown that the aerodynamic interaction with the carrier gas leads to an oblate shape, only partially compensate by the liquid circulation inside the drop that induces a deformation towards the prolate shape.
A drop travelling in a gaseous atmosphere is then subject to deformation [21] and oscillation [27] that to some extent may bring to drop break-up. The spherical drop turns out to be an idealisation that does not represent correctly the reality, although it allows a simpler approach to modelling.
In the last years, there was a growing interest in studying the possible effects of deformation on transport phenomena like heating and evaporation and some first attempts to relieve the above mentioned simplifying hypothesis can be found in the literature [21, 28-32]. These models were developed for single component drops and they are still to be assessed against experiments, owing to the difficulty in performing accurate measurements on deformed drops.
It is however of a certain theoretical and practical interest to study the effect of deformation on multicomponent drop evaporation, and the present paper is a first attempt in that direction. The following sections report an extension of a model for multicomponent spherical drops [12] (previously developed by the authors of the present paper) to model evaporation from deformed (ellipsoidal) multicomponent drops by applying a theoretical approach recently proposed by the same authors [31].

Model equations

The model described below is an extension of a previous one [12], developed for spherical multicomponent drops, to account for the effect of drop deformation on evaporation of multicomponent drops.
The theoretical approach developed in [31] is applied to solve the species conservation equations:

$$\nabla_j n_j^{(\alpha)} = 0 \quad \alpha = 0,1,...n \tag{1}$$

in a general orthogonal coordinate system. Assuming that Soret effect, pression diffusion, and other second order effects are neglectful (see [33] for more details), and assuming the Fick's law [33] as commonly accepted constitutive equation, the species flux vectors can be written as:

$$n_j^{(\alpha)} = \rho U_j \chi^{(\alpha)} - \rho D^{(\alpha,m)} \frac{1}{h_j} \frac{\partial \chi^{(\alpha)}}{\partial x^j} \tag{2}$$

where χ^k is the generic curvilinear coordinate and h_k is the the k^{th} scale factor.
Under uniform boundary conditions on the drop surface and at infinity, the vapour diffusion/convection is one-dimensional, and the conservation equations (1), accounting for equation (2) can be written in normalised basis:

$$\frac{\partial}{\partial \xi}\left\{ h_u h_v \rho U \chi^{(\alpha)} - \rho D^{(\alpha,m)} \frac{h_u h_v}{h_\xi} \frac{\partial \chi^{(\alpha)}}{\partial \xi} \right\} = 0 \tag{3}$$

where ξ is the coordinate normal to the drop. The drop surface is defined by the equation $\xi = \xi_0$, and h_u and h_v are the scale factors for the coordinates u,v along the surface, U is the ξ-component (the only non-nil component in a 1-D problem) of the Stefan velocity. The total mass conservation is obtained summing equations (1) on α from 0 to n, and in doing so it should be noticed that the Fick's law terms in equation (2) do not sum up to zero. This is due to the fact that Fick's law is an approximation that holds only for dilute components and then it is not expected to hold for the main (α=0) component. A more rigorous approach, based on Stefan-Maxwell equation as in [14], would eliminate this inconsistency. In the present treatment the correct form of the mass conservation equation is assumed and its integration yields:

$$\rho U = \frac{C(u,v)}{h_u h_v} \tag{4}$$

where $C(u,v)$ is an arbitrary function of u and v.

The analytical solution

Consider now the case when $h_\xi/(h_u h_v)$ is separable, i.e.:

$$\frac{h_\xi}{h_u h_v} = H(u,v) f(\xi) \tag{5}$$

that it was shown in [31] to be the sufficient condition for the existence of a 1-D solution. Equations (3), making use of equations (4) and (5), become:

$$H(u,v)C(u,v)\frac{\partial \chi^{(\alpha)}}{\partial \xi} = \rho D^{(\alpha,m)} \frac{\partial}{\partial \xi}\left(f(\xi)\frac{\partial \chi^{(\alpha)}}{\partial \xi} \right) \tag{6}$$

and since $\chi^{(\alpha)}$ must be function only of ξ:

$$H(u,v)C(u,v) = M_1 = const. \tag{7}$$

Integrating the species equations (6) yields the analytical solution:

$$\chi^{(\alpha)} = k^{(\alpha)} e^{\frac{M_1}{\rho D^{(\alpha,m)}}\int f(\xi)d\xi} + \gamma^{(\alpha)} \tag{8}$$

where k^α and $\gamma^{(\alpha)}$ are arbitrary constants, which can be found from the Dirichlet B.C.:

$$\chi^{(\alpha)}(\xi_0) = \chi_s^{(\alpha)}; \quad \chi^{(\alpha)}(\infty) = \chi_\infty^{(\alpha)} \tag{9}$$

yielding:

$$k^{(\alpha)} = \frac{\chi_s^{(\alpha)} - \chi_\infty^{(\alpha)}}{1 - e^{\frac{M_1}{\rho D^{(\alpha,m)}}\int_{\xi_0}^{\infty} f(\xi)d\xi}}; \quad \gamma^{(\alpha)} = \frac{\chi_s^{(\alpha)} - \chi_\infty^{(\alpha)} e^{\frac{M_1}{\rho D^{(\alpha,m)}}\int_{\xi_0}^{\infty} f(\xi)d\xi}}{1 - e^{\frac{M_1}{\rho D^{(\alpha,m)}}\int_{\xi_0}^{\infty} f(\xi)d\xi}} \tag{10}$$

The evaporation rate

The local vapour fluxes can be calculated from equations (2):

$$n_\xi^{(\alpha)} = \frac{M_1}{h_u h_v H(u,v)} \gamma^{(\alpha)} \tag{11}$$

and it can be easily shown that the constants $\gamma^{(\alpha)}$ are the evaporation rate fractions of the α-components. To notice that since the drop surface is still and it is assumed that the gas species (α=0) does not diffuse into the liquid, the mass flux $n_\xi^{(0)}$ is nil at the drop surface and then is nil everywhere, thus $\gamma^{(0)} = 0$.

The evaporation rate for each species can be calculated integrating the species flux over the drop surface, yielding:

$$m_{ev}^{(\alpha)} = M_1 \int \frac{dudv}{H(u,v)} \gamma^{(\alpha)} \tag{12}$$

and for the total evaporation rate:

$$m_{ev}^{(T)} = \sum_{\alpha=1}^{n} m_{ev}^{(\alpha)} = M_1 \int \frac{dudv}{H(u,v)} \sum_{\alpha=1}^{n} \gamma^{(\alpha)} = M_1 \int \frac{dudv}{H(u,v)} \tag{13}$$

since the condition:

$$\sum_{\alpha=1}^{n} \gamma^{(\alpha)} = 1 \tag{14}$$

holds. Equation (14), accounting for equations (10) and (13), is a nonlinear algebraic equation in the sole unknown $m_{ev}^{(T)}$, and its solution yields $m_{ev}^{(T)}$ and then, by equations (10), the partial mass flow rates.

The thermal problem

The heat transfer to the evaporating ellipsoidal drop was analysed in [31] and the following general equation to calculate the heat transfer rate was derived:

$$\dot{Q} = 4\pi R_0 k_{ref} \left(T_s - T_\infty\right) \left(\frac{Y e^{-Y\frac{R_0}{R_{eq}}}}{1 - e^{-Y\frac{R_0}{R_{eq}}}} \right) \tag{15}$$

where $Y = \dfrac{m_{ev}^{(T)} c_{p,ref}}{4\pi R_0 k_{ref}}$ and R_0 is the radius of a spherical drop having the same volume of the deformed one, i.e.:

$$R_0 = \left(\frac{3V}{4\pi} \right)^{1/3} \tag{16}$$

where V is the drop volume. The results of this analysis is independent of the fact that the total evaporation rate is made by a mixture of component rather that a single one, than equation (15) can be applied also to the present case.

Application to ellipsoidal drops

Following [31], the cases of spherical, spheroidal (oblate and prolate) and triaxial ellipsoidal drops can be treated in a unified way. Equation (14) can be re-written, accounting for equations (10) and (13) in a unique form:

$$1 = \sum_{\alpha=1}^{n} \frac{\chi_s^{(\alpha)} - \chi_\infty^{(\alpha)} e^{\frac{m_{ev}^{(T)}}{4\pi\rho D^{(\alpha,m)} R_{eq}}}}{1 - e^{\frac{m_{ev}^{(T)}}{4\pi\rho D^{(\alpha,m)} R_{eq}}}} \tag{17}$$

where:

$$\frac{1}{4\pi R_{eq}} = \frac{\int_{\xi_0}^{\infty} f(\xi) d\xi}{\int \frac{dudv}{H(u,v)}} \tag{18}$$

and the integrals depend only on the coordinate system and the following Table 1 (see [31]) yields the values of R_{eq} corresponding to the above mentioned drop shapes.

Table 1. Values of R_{eq}/R_0 for ellipsoidal drops of different kind.

Shape	$\varepsilon_y = \frac{a_y}{a_x}$	$\varepsilon_z = \frac{a_z}{a_x}$	$\frac{R_{eq}}{R_0}$
Sphere	1	1	1
Prolate	$\frac{1}{\varepsilon}$	$\frac{1}{\varepsilon} < 1$	$\frac{\left\|1-\varepsilon^2\right\|^{1/2}}{\varepsilon^{1/3}} \frac{1}{ln\left(\sqrt{\frac{\varepsilon+1}{\varepsilon-1}}-1\right) - ln\left(\sqrt{\frac{\varepsilon+1}{\varepsilon-1}}+1\right)}$
Oblate	1	$\varepsilon < 1$	$\frac{\left\|1-\varepsilon^2\right\|^{1/2}}{\varepsilon^{1/3}} \frac{1}{\pi - 2\,arctan\left(\sqrt{\frac{1+\varepsilon}{1-\varepsilon}}\right)}$
Triaxial	$\varepsilon_y < 1$	$\varepsilon_z < 1$	$\frac{\left\|1-\varepsilon_z^2\right\|^{1/2}}{\left(\varepsilon_y \varepsilon_z\right)^{1/3}} \frac{1}{F\left(\sqrt{1-\varepsilon_z^2}, \sqrt{\frac{1-\varepsilon_y^2}{1-\varepsilon_z^2}}\right)}$

In Table 1 $F(x,k)=\int_0^x \frac{dt}{\sqrt{1-k^2t^2}\sqrt{1-t^2}}$ is the incomplete elliptic integral of first kind (see [34]), and $a_x \geq a_y \geq a_z$ (see Figure 1) are the ellipsoid half-axes, that for a sphere are equal to R_0, whereas for the spheroids they satisfy the relation:

$$\begin{matrix} a_x = a_y \geq a_z & \text{oblate} \\ a_x \geq a_y = a_z & \text{prolate} \end{matrix} \quad (19)$$

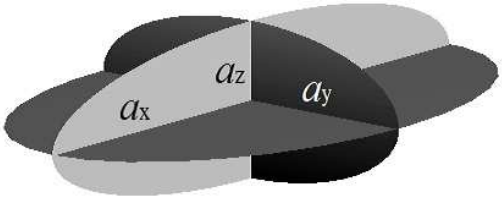

Figure 1. Definition of the ellipsoid half-axes

It must be noticed that $m_{ev}^{(T)} / R_{eq}$ is evaluated solving equation (17) and it does not depend on drop shape, then the evaporation rate fractions (10) do not depend on drop shape either, although clearly $m_{ev}^{(T)}$ does.

Evaporation under convective conditions

The above developed model holds for a drop floating in a quiescent gaseous environment, but a deformed drop under such condition cannot maintain its shape and undergoes shape oscillation. The evaporation from a single component oscillating drop was modelled on the basis of a theoretical approach similar to the one used in (see [35]. However, a liquid drop can assume a deformed shape when is travelling in a gas due to aerodynamics interaction at $\mathrm{Re}>0$ and the oblate shape is an acceptable approximation of the real drop shape under such conditions (see [28]).

To extend the present model to $\mathrm{Re}>0$ conditions, an approach similar to that developed in [5] for single component and extended in [12] for multicomponent droplet, based on film theory [36], will be adopted. This approach assumes that the evaporating drop is surrounded by different mass diffusional regions, which thicknesses may depend on the physical properties of each vapour species. Under such assumption the evaporation rate of each species under convective ($\mathrm{Re}>0$) conditions can be related to the one evaluated at $\mathrm{Re}=0$ by a semi-empirical rule (see [12]):

$$m_{ev,c}^{(\alpha)} = \frac{Sh^{(\alpha)}}{2} m_{ev}^{(\alpha)} \quad (20)$$

where the Sherwood number for each species $Sh^{(\alpha)}$,following [5] and [12], is found by semi-empirical correlations:

$$Sh^{(\alpha)} = 2 + \frac{Sh_0^{(\alpha)} - 2}{F_M\left(B_M^{(m)}\right)} \quad (21)$$

$$Sh_0^{(\alpha)} = 2 + 0.55\,\mathrm{Re}^{1/2}\, Sc_\alpha{}^{1/3} \quad (22)$$

$$F_M(x) = \frac{(1+x)^{0.7}\, ln(1+x)}{x} \quad (23)$$

being $Sc_{(\alpha)}=\nu/D^{(\alpha,m)}$ the Schmidt number for the species α, and the mass transfer number for the gaseous mixture is defined as follows [12]:

$$B_M^{(m)} = \frac{\sum_{\alpha=1}^{n} \chi_s^{(\alpha)} - \sum_{\alpha=1}^{n} \chi_\infty^{(\alpha)}}{1 - \sum_{\alpha=1}^{n} \chi_s^{(\alpha)}} \quad (24)$$

As a consequence, the drop total evaporation rate under convective conditions ($m_{ev,c}^{(T)}$) can be simply correlated to the total evaporation rate ($m_{ev}^{(T)}$) and evaporation rate fractions ($\gamma^{(\alpha)}$) under non convective conditions:

$$m_{ev,c}^{(T)} = \frac{\sum_{\alpha=1}^{n} Sh^{(\alpha)}\gamma^{(\alpha)}}{2} m_{ev}^{(T)} \tag{25}$$

The evaporation rate fraction for each species under convective conditions $\beta_c^{(\alpha)}$ can then be calculated as :

$$\beta_c^{(\alpha)} = \frac{Sh^{(\alpha)}\gamma^{(\alpha)}}{\sum_{k=1}^{n} Sh^{(k)}\gamma^{(k)}} \tag{26}$$

A similar procedure is followed to evaluate the heat rate to the drop. The heat rate under convective conditions can be written as:

$$\dot{Q} = 2\pi R_0 k_{ref} Nu^* \left(T_s - T_\infty\right) \left(\frac{Ye^{-Y\frac{R_0}{R_{eq}}}}{1-e^{-Y\frac{R_0}{R_{eq}}}} \right) \tag{27}$$

where, following [5] :

$$Nu^* = 2 + \frac{Nu_0 - 2}{F_M\left(B_T\right)} \tag{28}$$

$$Nu_0 = 2 + 0.55\,\mathrm{Re}^{1/2}\,\mathrm{Pr}^{1/3} \tag{29}$$

and:

$$B_T = \left(1 + B_M^{(m)}\right)^{\Phi} - 1 \qquad \Phi = \frac{c_{p,ref}}{c_p^{(0)}} \frac{Sh^*}{Nu^*} \frac{1}{Le} \tag{30}$$

where $Sh^* = \sum_{\alpha=1}^{n} Sh^{\alpha}\gamma_c^{(\alpha)}$, $Le = k_{ref} \big/ c_{p,ref}\rho_{ref} D_{ref}$ and $D_{ref} = \sum_{\alpha=1}^{n} D_{ref}^{(\alpha,n)} \chi_{ref}^{(\alpha)} \Big/ \sum_{\alpha=1}^{n} \chi_{ref}^{(\alpha)}$.

Results and Discussion

This section reports the results from the parametrical analysis of the proposed multicomponent model, made to enlighten the effect of drop shape on the evaporation characteristics, under different operating conditions. The effects of initial drop size and temperature, gas temperature and convective conditions on the temporal variation of drop volume and liquid temperature have been investigated. The liquid mixture used in the following analysis is made by 50% ethanol and 50% acetone, as in [37]. For all the test cases considered in this section, the vapour concentrations are assumed equal to zero at free stream conditions (i.e. $\chi_\infty^{(\alpha)} = 0$) .

Initially, the effect of drop deformation has been analysed under quasi-steady conditions. The instantaneous evaporation rate of liquid drops having the same mass and different shapes is calculated. The drop temperature is fixed equal to 300K, while the gas phase is assumed stagnant at 500K and 1bar. Figure 2 shows the non-dimensional instantaneous evaporation rate $Y^{(\alpha)}$ defined as:

$$Y^{(\alpha)} = \frac{m_{ev}^{(\alpha)} c_{p,ref}}{4\pi R_0 k_{ref}} \tag{31}$$

for the two species (ethanol and acetone) as function of the drop surface area non-dimensionalised by the surface of a spherical drop having the same volume ($\beta = A_{drop} \big/ 4\pi R_0^2$). The spheroidal cases of oblate and prolate drops are reported, for β ranging from 1 up to 1.5, which corresponds to ε varying from 1 up to about 0.22 for the oblate shape and ε varying from 1 up to about 7 for the prolate shape. The figure confirms the increase of the evaporation rate as the drop surface increases and, for any given value of drop surface, the evaporation rate of the prolate drop is always higher than that of the corresponding oblate drop. To be noticed that the evaporation rate for any triaxial ellipsoidal drops with the same surface area ratio β lays between the two spheroidal test cases, as shown in [31]. For the oblate drop with β equal to 1.4, which corresponds to a value of ε equal to 0.25, the increase of the evaporation rate compared to the spherical case is about 16%, while for the corresponding prolate drop is about 28%, independently of the vaporising species.

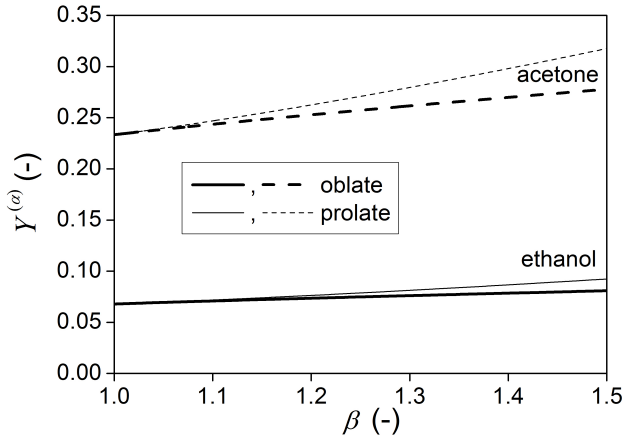

Figure 2. Effect of drop shape on non-dimensional instantaneous evaporation rate $Y^{(\alpha)}$ for ethanol and acetone, as function of the non-dimensional drop surface area, for a mixture of 50% ethanol and 50% acetone, T_s=300K, T_∞=500K, Re=0.

The following analysis considers the effect of drop shape under transient conditions, and the hypothesis of infinite liquid thermal conductivity is imposed, then an homogeneous drop temperature is assumed.
The comparison between a spherical and an oblate (with ε equal to 0.25) drop having the same volume is proposed, varying the drop initial dimension and temperature, the gas temperature and liquid/gas relative velocity. The choice to select an oblate drop is motivated by the findings from literature, which reports that drop floating in a moderate convective environment usually attain an oblate shape [28].
Figure 3 shows the transient profiles of the non-dimensional drop volume (defined as the ratio between the drop volume and its value at the initial time) and liquid temperature for drops vaporising in a stagnant environment (Re=0) made of air at 500K and 1 bar. The drop initial temperature is fixed equal to 300K, while three initial radius have been selected equal to 5, 10 and 25μm. For the oblate shape, the drop radius is assumed as the 'equivalent' drop radius of a spherical drop having the same volume of the oblate drop. The x-axis for all the graphs reports the non-dimensional time, calculated as follows:

$$\tau = \frac{tD_v^{(nom)}}{R_0^2} \tag{32}$$

where $D_v^{(nom)}$ is a 'nominal' mass diffusion coefficient calculated for the mixture of 50%ethanol-50%acetone in air as $D_v^{nom} = \sum D_{Tref}^{(\alpha,m)} \chi_{Tref}^{(\alpha)} / \sum \chi_{Tref}^{(\alpha)}$ (see also [12]), using as reference temperature T_{ref}=367K.

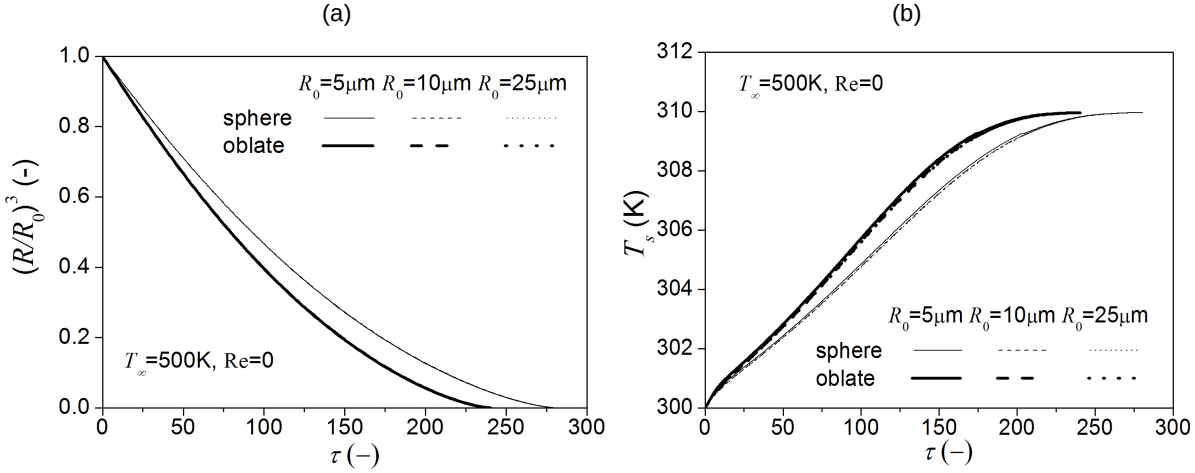

Figure 3. Effect of drop shape and initial drop size on (a) non-dimensional volume and (b) liquid temperature transient profiles for a bi-component drop, T_s=300K, T_∞=500K, Re=0.

The graph of figure 3(a) shows that the instantaneous drop volume and temperature are almost perfectly scaled by the choice of the non-dimensional time τ, for both the drop shapes. The comparison between the two drop shapes evidences that the increase of drop surface due to the deformation have a relevant effect on the drop lifetime (calculated when the drop size reduces to about 1% of the initial drop radius), which reduces of about 14.3% compared to the spherical case, almost independently of the initial drop size. Figure 3(b) shows the liquid

temperature transient profiles for the six cases of figure 3(a). All the cases are characterised by a monotonic increase of the drop temperature along the whole drop lifetime, attaining a quasi-asymptotic liquid temperature towards the end of the vaporisation process, i.e. when the lighter component is almost totally vaporised and the liquid composition is almost mono-component.

The steeper increase of drop temperature for the oblate case can be explained observing that for the oblate case both the sensible heat rate, which is proportional to the gas-drop temperature difference (equation 15), and the latent heat rate, which is the product between the evaporation rate and the latent heat of vaporisation, increases of the same amount, thus increasing the steepness of the temperature profile. When the drop (oblate and spherical) reach the asymptotic temperature, the latent and sensible heat rates almost perfectly balance each other, without any detectable effect on the gas-drop temperature difference, since both effects are purely driven by the drop deformation (increase of surface area and change of curvature), thus explaining the fact that the asymptotic temperature is almost independent of the drop shape.

This phenomenon is confirmed in the following figure 4, which reports the temporal profiles of the non-dimensional volume and liquid temperature, for the same test cases of figure 3, but increasing the gas temperature up to 1000K. Figure 4(a) shows the same behaviour of figure 3(b), with the drop volume almost perfectly scaled with the drop size, independently of the drop shape. Clearly the increase of gas temperature accelerates the evaporation for all the test cases, and the lifetime of the oblate drops is again lowered by about 14.2 %, for all drop sizes.

The graph of figure 4(c) presents now a different behaviour, compared to the lower gas temperature case (figure 3b). The liquid temperature initially experiences a marked increase, then the slope of the drop temperature reduces until the reaching of a quasi-stationary value. Also in this case, the oblate drops have a higher temperatures compared to the spherical ones, but they reach the same asymptotical temperature.

The difference of the initial temperature slopes for the two cases reported in figure 3(b) and 4(b) are related to the relative value of the drop initial temperature compared to the gas temperature.

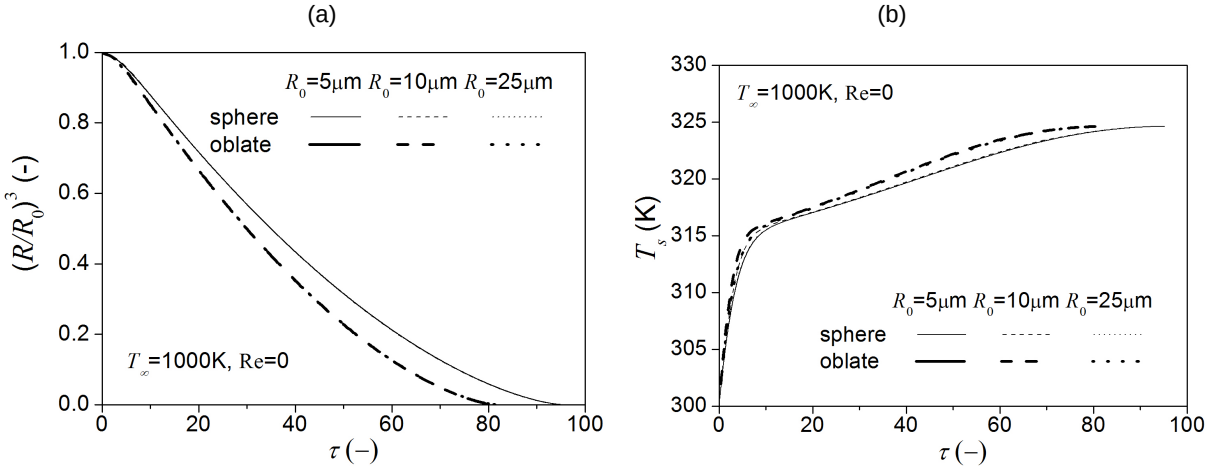

Figure 4. Effect of drop shape and initial drop size on (a) non-dimensional volume and (b) liquid temperature transient profiles for a bi-component drop, T_s=300K, T_∞=1000K, Re=0.

Figure 5 reports the transient temperature profiles for spherical and oblate drops with initial radius equal to 10μm, vaporising in stagnant air (Re=0) at 500K, fixing the initial drop temperature equal to 295, 300 and 305K. The graph evidenced that the initial reduction or rapid increase of drop temperature only depends on the instantaneous difference between the gas and liquid temperatures.

When the initial drop temperature is relatively high (ex. $T_{s,0}$=305K), both drop shapes experiences this phenomenon, which is due to the fact that at the initial stage of evaporation the latent heat rate is greater than the sensible heat rate . As the evaporation proceeds, the evaporation rate reduces (due to the lowering of the liquid temperature) then there is a point where the latent heat equals the sensible heat (which corresponds to the instant when the minimum liquid temperature is reached). From this point, the drop has a temperature that corresponds to a sensible heat always higher than the latent heat and the monotonic increase of liquid temperature is shown.

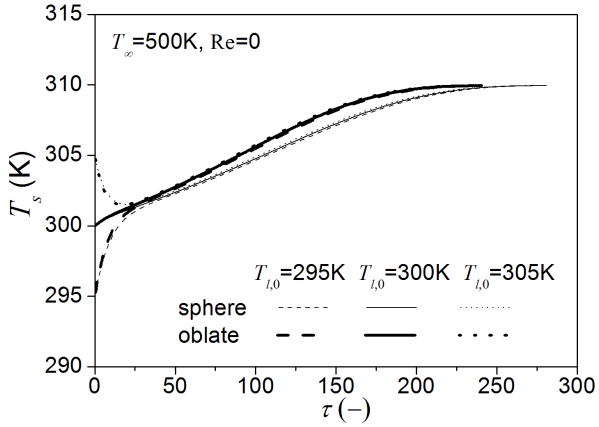

Figure 5. Effect of drop shape and initial drop temperature on liquid temperature transient profiles for a bi-component drop, R_0=10μm, T_∞=500K, Re=0.

The following graphs report the effect of convection on the evaporation characteristics for spherical and oblate drops. Figure 6 shows the transient profiles of non-dimensional drop volume and liquid temperature for spherical and oblate drop with initial equivalent radius equal to 10μm, vaporising in air at 500K. The drop/gas relative velocity, U_0, is fixed, through the whole drop lifetime, equal to 0, 10 and 20m/s, with the initial Reynolds number equal to 0, 7.8 and 15.6, respectively.

The presence of convective heat and mass transfer introduces a new effect that destroys the almost perfect scaling of the phenomena by the non-dimensional time τ. The drop lifetime reduces increasing Re, which increases the evaporation rate for both shapes (induced by the increased Sherwood number).

However, the lifetime reduction of the oblate drop relative to the spherical one is still around 14.3%, almost independently of the Reynolds number.

To be noticed that now, with U_0 equal to 10 and 20m/s, all drops experience the initial liquid temperature reduction, due to the increased latent heat rate (induced by the increased Sherwood number), which is not compensated by the increase of the sensible heat rate (induced by the increased Nusselt number).

Figure 7 shows the same test cases of figure 6, increasing the gas temperature up to 1000K. The reduction of the drop lifetime for the oblate drop, compared to spherical, is again around 14.3%, almost independently of the convective conditions, but (see figure 6 b) the initial drop temperature reduction is substituted by and initial steep increase.

These results evidence that the drop deformation, increasing the instantaneous evaporation rate due to the increased surface area, accelerate the drop evaporation, although toward the end of the process the same asymptotic temperature is reached, owing to the coupling between heat and mass transfer phenomena.

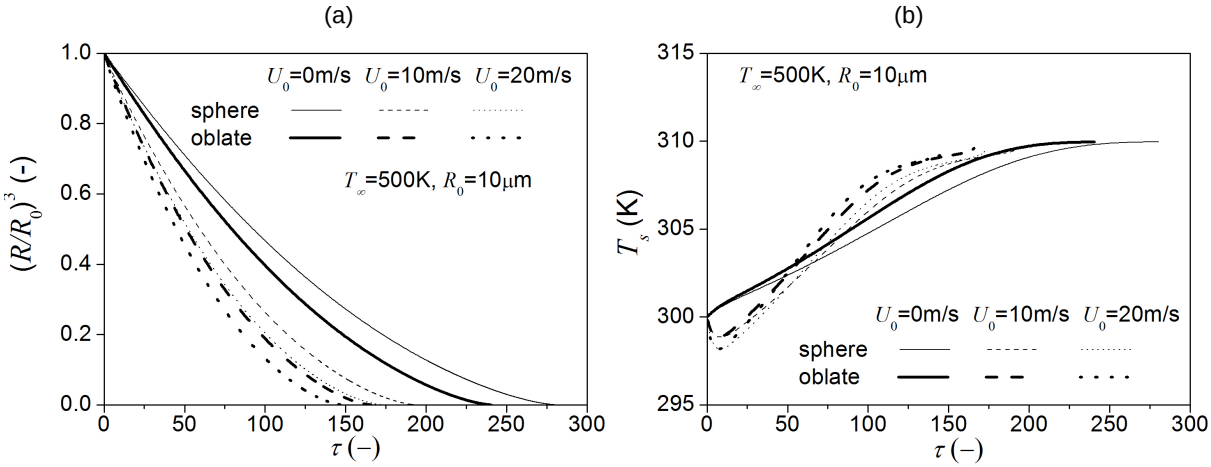

Figure 6. Effect of drop shape and initial drop velocity on (a) non-dimensional volume and (b) liquid temperature transient profiles for a bi-component drop, R_0=10μm, T_s=300K, T_∞=500K.

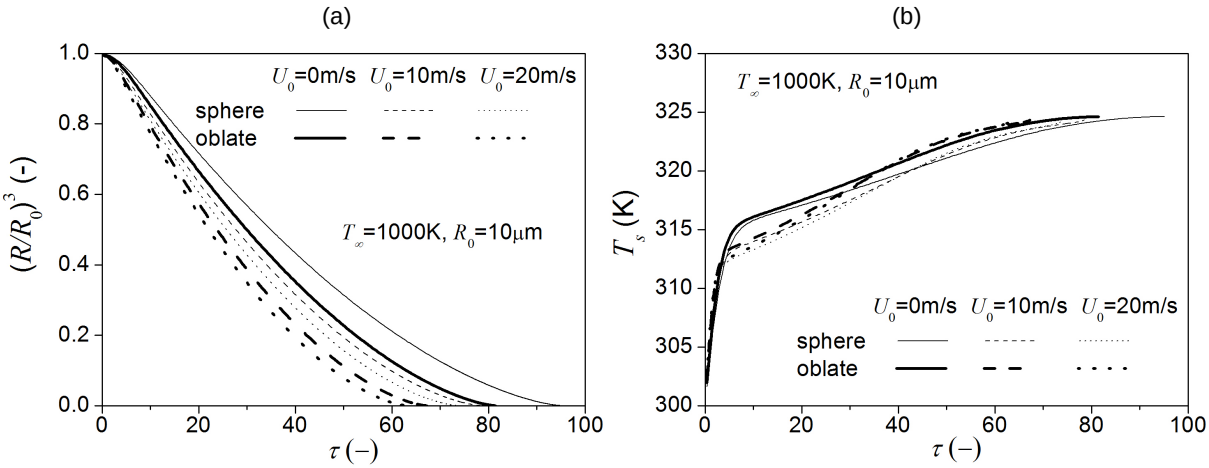

Figure 7. Effect of drop shape and initial drop velocity on (a) non-dimensional volume and (b) liquid temperature transient profiles for a bi-component drop, R_0=10μm, T_s=300K, T_∞=1000K.

Conclusions

A model for heating and evaporation of non-spherical multicomponent drops was developed, extending a model, previously developed by the same authors, for multicomponent spherical drop to ellipsoidal drops through the solution of energy and species conservation equations in orthogonal curvilinear coordinates. The case of ellipsoidal (triaxial, prolate and oblate spheroids) drops is reported. The present analysis also extends the model developed (by the same authors) for single component ellipsoidal drops to convective conditions.

The model allows to evaluate the heat rate and the species evaporation rates through the solution of a single non-linear algebraic equation. The effect of deformation on the instantaneous evaporation rates of each single species was evaluated as a function of drop surface area, showing that a prolate drop experiences the largest evaporation rate compared to other ellipsoidal drops of the same volume and surface area.

An example of application to a double component oblate drops is reported, studying the drop size and the temperature evolution, for a range of drop size and temperature, gas temperature and drop-gas relative velocity.

It is found that the deformed drop attains the same asymptotic temperature but in a shortest time compared to the spherical case, almost independently of the drop size. The effect is enhanced by the increase of gas temperature and Reynolds number.

The coupling of heat and mass transfer phenomena causes a reduction of the oblate drop lifetime (of about 14% for this particular drop composition), compared to the spherical one, almost independently of the initial drop size, gas temperature, initial drop temperature and Reynolds number.

Nomenclature

a_x, a_y, a_z	ellipsoid half-axes [m^2]
B_M,B_T	Spalding mass and heat transfer numbers [-]
c_p	specific heat [J/kg K]
C	arbitrary function of u and v, equation (4) [-]
D	diffusion coefficient [m^2/s]
f	function of ξ, equation (5) [-]
$F(x,k)$	incomplete elliptic integral of first kind [-]
F_M	non-dimensional function, equation (23) [-]
h	scale factors [m]
H	function of u and v, equation (5) [-]
m_{ev}	evaporation rate [kg/s]
M_1	constant, equation (7) [-]
n	vapour flux [kg/m^{2}s]
Nu	Nusselt number [-]
Pr	Prandtl number [-]
$\dot{Q}$	heat rate [W]
Re	Reynolds number [-]
R_{eq}	deformation length, equation (18) [m]
R_0	equivalent drop radius [m]
Sc	Schmidt number [m]

Sh	Sherwood number [-]
T	temperature [K]
u,v	curvilinear coordinates along the drop surface [-]
U	Stefan velocity [m/s]
U_0	drop-gas relative velocity [m/s]
V	volume [m^3]
Y	non-dimensional evaporation rate [-]
Greek symbols	
β	non-dimensional drop surface area [-]
γ	evaporation rate fractions [-]
ε	drop deformation parameter, Table 1 [-]
ξ	curvilinear coordinate [-]
ρ	mass density [kg/m^3]
Φ	non-dimensional parameter, equation (30) [-]
τ	non-dimensional time [-]
χ	species mass fraction [-]
Superscripts	
m	mixture
nom	nominal
α	vapour species
$*$	modified
Subscripts	
c	convective
l	liquid
ref	reference conditions
s	at drop surface
∞	at infinity

References

[1] Sazhin, S., 2014, Droplets and Sprays, Springer.
[2] Sirignano, W. A., and Mehring, C., 2000, "Review of theory of distortion and disintegration of liquid streams," Progress in Energy and Combustion Science, 26(4), pp. 609-655.
[3] Maxwell, J. C., 1878, "Diffusion," Encyclopedia britannica, 7, pp. 214-221.
[4] Fuchs, N. A., 1959, Evaporation and droplet growth in gaseous media, Pergamon Press.
[5] Abramzon, B., and Sirignano, W. A., 1989, "Droplet vaporization model for spray combustion calculations," Int. J. Heat Mass Tran., 32(9), pp. 1605-1618.
[6] Nikolopoulos, N., Theodorakakos, A., and Bergeles, G., 2007, "A numerical investigation of the evaporation process of a liquid droplet impinging onto a hot substrate," Int. J. Heat Mass Tran., 50(1), pp. 303-319.
[7] Strotos, G., Gavaises, M., Theodorakakos, A., and Bergeles, G., 2011, "Numerical investigation of the evaporation of two-component droplets," Fuel, 90(4), pp. 1492-1507.
[8] Brenn, G., Deviprasath, L. J., Durst, F., and Fink, C., 2007, "Evaporation of acoustically levitated multi-component liquid droplets," Int. J. Heat Mass Tran., 50(25), pp. 5073-5086.
[9] Sazhin, S. S., Elwardany, A. E., Krutitskii, P. A., DeprÃ©durand, V., Castanet, G., Lemoine, F., Sazhina, E. M., and Heikal, M. R., 2011, "Multi-component droplet heating and evaporation: numerical simulation versus experimental data," Int. J. Therm. Sci., 50(7), pp. 1164-1180.
[10] Sazhin, S. S., Shishkova, I. N., and Al Qubeissi, M., 2014, "Heating and evaporation of a two-component droplet: Hydrodynamic and kinetic models," Int. J. Heat Mass Tran., 79, pp. 704-712.
[11] Tong, A. Y., and Sirignano, W. A., 1986, "Multicomponent transient droplet vaporization with internal circulation: integral equation formulation and approximate solution," Numer. Heat Tr. a-Appl., 10(3), pp. 253-278.
[12] Tonini, S., and Cossali, G. E., 2015, "A novel formulation of multi-component drop evaporation models for spray applications," Int. J. Therm. Sci., 89, pp. 245-253.
[13] Zhang, L., and Kong, S.-C., 2012, "Multicomponent vaporization modeling of bio-oil and its mixtures with other fuels," Fuel, 95, pp. 471-480.
[14] Tonini, S., and Cossali, G. E., 2015, "A multi-component drop evaporation model based on analytical solution of Stefan-Maxwell equations," International Journal of Heat and Mass Transfer, 92, pp. 184-189.
[15] Maqua, C., Castanet, G., and Lemoine, F., 2008, "Bicomponent droplets evaporation: Temperature measurements and modelling," Fuel, 87(13), pp. 2932-2942.
[16] Wilms, J., 2005, "Evaporation of multicomponent droplets,"PhD Thesis, Universität Stuttgart.

[17] Stengele, J., Prommersberger, K., Willmann, M., and Wittig, S., 1999, "Experimental and theoretical study of one-and two-component droplet vaporization in a high pressure environment," International journal of heat and mass transfer, 42(14), pp. 2683-2694.
[18] Elwardany, A. E., and Sazhin, S. S., 2012, "A quasi-discrete model for droplet heating and evaporation: application to Diesel and gasoline fuels," Fuel, 97, pp. 685-694.
[19] Sazhin, S. S., Al Qubeissi, M., Nasiri, R., Gun'ko, V. M., Elwardany, A. E., Lemoine, F., Grisch, F., and Heikal, M. R., 2014, "A multi-dimensional quasi-discrete model for the analysis of Diesel fuel droplet heating and evaporation," Fuel, 129, pp. 238-266.
[20] Sazhin, S. S., Al Qubeissi, M., Kolodnytska, R., Elwardany, A. E., Nasiri, R., and Heikal, M. R., 2014, "Modelling of biodiesel fuel droplet heating and evaporation," Fuel, 115, pp. 559-572.
[21] Mashayek, F., 2001, "Dynamics of evaporating drops. Part I: formulation and evaporation model," Int. J. Heat Mass Tran., 44(8), pp. 1517-1526.
[22] Haywood, R. J., Renksizbulut, M., and Raithby, G. D., 1994, "Transient deformation and evaporation of droplets at intermediate Reynolds numbers," Int. J. Heat Mass Tran., 37(9), pp. 1401-1409.
[23] Loth, E., 2008, "Quasi-steady shape and drag of deformable bubbles and drops," Int. J. Multiphase Flow, 34(6), pp. 523-546.
[24] Hase, M., and Weigand, B., 2004, "Transient heat transfer of deforming droplets at high Reynolds numbers," International Journal of Numerical Methods for Heat & Fluid Flow, 14(1), pp. 85-97.
[25] Schlottke, J., and Weigand, B., 2008, "Direct numerical simulation of evaporating droplets," Journal of Computational Physics, 227(10), pp. 5215-5237.
[26] Helenbrook, B. T., and Edwards, C. F., 2002, "Quasi-steady deformation and drag of uncontaminated liquid drops," Int. J. Multiphase Flow, 28(10), pp. 1631-1657.
[27] Mashayek, F., 2001, "Dynamics of evaporating drops. Part II: free oscillations," Int. J. Heat Mass Tran., 44(8), pp. 1527-1541.
[28] Bakhshi, A., Ganji, D. D., and Gorji, M., 2015, "Deformation and Breakup of an Axisymmetric Falling Drop under Constant Body Force," International Journal of Partial Differential Equations and Applications, 3(1), pp. 1-6.
[29] Sanyal, A., Basu, S., and Kumar, R., 2014, "Experimental analysis of shape deformation of evaporating droplet using Legendre polynomials," Physics Letters A, 378(5), pp. 539-548.
[30] Tonini, S., and Cossali, G. E., 2013, "An exact solution of the mass transport equations for spheroidal evaporating drops," Int. J. Heat Mass Tran., 60, pp. 236-240.
[31] Tonini, S., and Cossali, G. E., 2016, "One-dimensional analytical approach to modelling evaporation and heating of deformed drops," International Journal of Heat and Mass Transfer, 97, pp. 301-307.
[32] Li, J., and Zhang, J., 2014, "A theoretical study of the spheroidal droplet evaporation in forced convection," Physics Letters A, 378(47), pp. 3537-3543.
[33] Slattery, J. C., 1981, Momentum, energy and mass transfer in continua,, R. Krieger Publ.
[34] Olver, F. W. J., Lozier, D. W., Boisvert, R. F., and Clark, C. W., 2010, NIST Handbook of Mathematical Functions, Cambridge University Press.
[35] Tonini, S., and Cossali, G. E., 2014, "An evaporation model for oscillating spheroidal drops," Int. Commun. Heat Mass, 51, pp. 18-24.
[36] Bird, R. B., Stewart, W. E., and Lightfoot, E. N., 2002, Transport Phenomena, Wiley, New York
[37] Sazhin, S. S., Elwardany, A., Krutitskii, P. A., Castanet, G., Lemoine, F., Sazhina, E. M., and Heikal, M. R., 2010, "A simplified model for bi-component droplet heating and evaporation," Int. J. Heat Mass Tran., 53(21), pp. 4495-4505.